Digest Journal of Nanomaterials and Biostructures Vol. 18, No. 4, October-December 2023, p.1599-1611

Effect of $NiFe_2O_4$ contents on the structural, optical and electrical properties of PEO/CMC-$NiFe_2O_4$ nanocomposite

L. H. Gaabour[a,*], S. K. Alghamdi[b]
[a]*University of Jeddah, College of Science, Department of Physical Sciences, Jeddah, Saudi Arabia*
[b]*Physics Department, Faculty of Sciences, Taibah University, Saudi Arabia*

In this study the casting method was used to prepare new polymeric nanocomposites by filling a polymer blend based on polyethylene oxide (PEO) and carboxymethyl cellulose (CMC) by adding different calculated weight ratios of nickel ferrite nanoparticles ($NiFe_2O_4$) which were prepared by solvothermal technique. The XRD and ATR-FTIR measurements confirmed the formation of $NiFe_2O_4$ NPs, and the transmission electron microscope (TEM) showed that $NiFe_2O_4$ NPs have a semispherical shape. The ATR-FTIR and XRD affirmed the miscibility and complexation between a pure blend of PEO/CMC and PEO/CMC-$NiFe_2O_4$ nanocomposites. Significant structural, optical, and morphological changes were seen in PEO/CMC/$NiFe_2O_4$ nanocomposites. These changes, in turn, caused a shift in the absorption edge toward a lower wavelength, which resulted in a drop in the energy gap value. The AC electrical conductivity (σ_{ac}), dielectric constant (ε'), dielectric loss (ε''), and the dielectric moduli (M' and M").

(Received September 20, 2023; Accepted December 18, 2023)

Keywords: PEO/CMC, $NiFe_2O_4$ NPs, Solvothermal method, Dielectric studies

1. Introduction

It has become common in scientific research now to blend between two or more polymers to obtain a new advanced polymeric material that combines the physical, structural, and chemical properties of the two polymers compared to a single polymer [1, 2]. Researchers in applied domains have noticed this synthesis approach because of its attractive combination of simplicity and cost. The qualities of the final product are affected by several variables, such as the mixing technique, the ratio of polymers used, the temperature used to mix, and the degree of mixing [3]. The formation of interfacial contacts between the functional groups within the two polymers has a significant impact on the polymer blending process used as well as the outstanding properties of the final material. In addition, the insertion of nanomaterials into the polymeric mixture works to improve and modify the properties of the composites formed as a result of the interaction and bonding that occurs between the functional groups of the polymer with the ions of the added nanoparticles.

The resultant polymer nanocomposite exhibits vastly enhanced electrical, dielectric, optical, and thermal characteristics [4-6]. PEO can interact with the cations of numerous metal salts attributed to the manifestation of an ether group (C-O-C) in its chemical structure, which is one of the reasons why it is beneficial for supporting fast ion transport. Because carboxymethyl cellulose (CMC) contains OH groups, it can interact with other polymers by establishing hydrogen bonds. CMC is both anionic and water-soluble [7, 8]. PEO also increases the product's mechanical qualities, and CMC boosts the amorphous aspect of the blend, which in turn raises the product's electrical conductivity [9].

Furthermore, both polymers are safe for human consumption, widely distributed, and inexpensive, adding to their potential candidates to be used in a wider range [10, 11]. Due to their extensive technological applications, the physical properties of nanoparticle materials have gained increased attention in recent years. Several studies are looking at how nanoparticles are distributed

* Corresponding author: Lhgaabour@uj.edu.sa
https://doi.org/10.15251/DJNB.2023.184.1599

throughout a polymer or polymer blend. Polymeric materials can benefit from incorporating nanoparticles in many ways, including those that have to do with the materials' composition, the number of nanoparticles used, the particles' sizes, and their uniformity [12, 13]. Nickel ferrite nanoparticles ($NiFe_2O_4$ NPs) have attracted great interest among many types of spinel iron, due to their increased magnetic loss and hysteresis loss absorption process, domain wall resonance, and natural resonances. These factors combine to make $NiFe_2O_4$ an exciting material. It has a low coercively and high saturation magnetization (Ms), making it excellent magnetic semiconducting material. Therefore, it has many possible uses, including adsorption, gas electromagnetic, sodium-ion batteries, magnetic separation of dye, wave absorption materials, boosting the water oxidation process, photocatalysis, etc. [14, 15]. In light of the preceding information, the main purpose of the present research is to determine the effect of different contents of $NiFe_2O_4$ NPs on the structural, optical, morphological, and dielectric properties of the PEO/CMC polymer blend.

2. Experimental work

Polyethylene oxide (PEO) with M.W. = 600,000 was supplied from ACROS Organics, while carboxymethyl cellulose (CMC) with M.W.= 250. 000 was purchased from BDH Company. Nickel chloride ($NiCl_2.6H_2O$), Ferric chloride ($FeCl_3.6H_2O$), ammonium hydroxide solution (NH_4OH, 28% NH_3 in H_2O), and ethylene glycol were provided by Sigma Aldrich Company.

A straightforward solvothermal approach was utilized throughout the manufacturing process of $NiFe_2O_4$ NPs. In a typical synthesis technique, the precursor salts, $NiCl_2.6H_2O$ and $FeCl_3.6H_2O$, with a molar ratio of 1:2, were added to a specific volume (75 mL) of Ethylene glycol while the mixture was vigorously stirred. After the solution became clear, Ammonia solution was added while stirring was maintained until pH equal to 12. Following 30 minutes of vigorous stirring, the liquid was moved to a Teflon-lined stainless steel autoclave and sealed. The temperature was then kept at 200 ºC for 48 hours. The temperature of the system returned to normal after being cooled down naturally. The brownish color precipitate was washed with pure C_2H_5OH and pure water and then dried at a temperature of 80 ºC for 12 hours.

Using the casting procedure as shown in Scheme 1. the created nanocomposite films from a pure PEO and CMC were prepared at a ratio of 50:50 wt./wt., containing different concentrations of $NiFe_2O_4$. They then mix the solutions at 50 º C for 6 hours to ensure a consistent blend. The next step involved adding an aqueous $NiFe_2O_4$ NPs solution to the blend at various filling levels (x = 4, 6, 10, and 15 wt%) and sonicated very well for 15 min to ensure the complete suspension inside PEO/CMC chains. After that, the nanocomposite solutions were cast into glass plates and dried at 48 ºC about 36 hours.

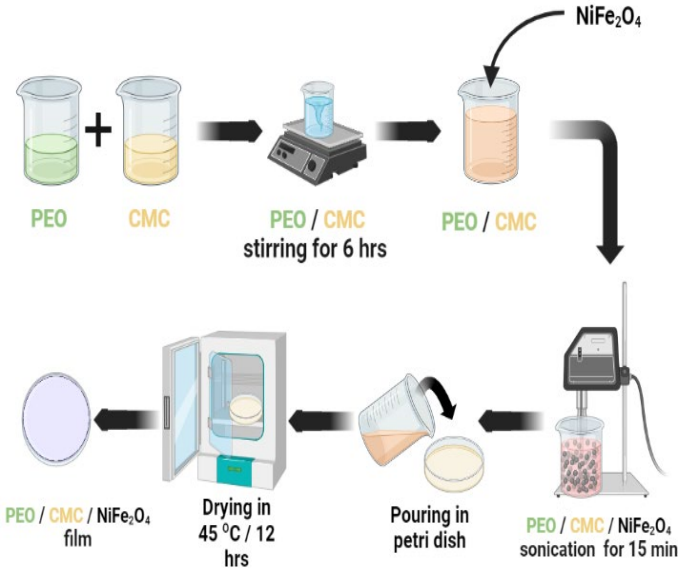

Scheme 1. Steps of preparation of PEO/CMC/ $NiFe_2O_4$ NPs.

The Vertex 80 Bruker was utilised to measure ATR-FTIR to conduct the comparative assessment of the produced nanocomposite films. The X-ray diffraction was taken using a PANalytical X'Pert Pro diffractometer with 2θ = 5°-60°. Ultraviolet–Visible (UV-Vis) measurements using a Jasco V-630 in the region of wavelength from 200-1000 nm. The size and shape of the $NiFe_2O_4$ NPs were measured using the transmission electron microscope (TEM), JEM-2100F electron microscope operating at 50 kV. The morphology of the samples was obtained by FESEM; Quanta 250 FEG. The dielectric parameters studies used broadband dielectric spectroscopy at the frequency range from 0.1 Hz to 10^{7} Hz.

3. Results and discussion

3.1. The ATR-FTIR analysis

Fig. 1. depicts the ATR-FTIR spectra of the pure PEO, CMC and nickel ferrite nanoparticles ($NiFe_2O_4$) in the range of wavenumber 4000-400 nm. The spectrum (a) of pure PEO display the IR bands that appeared at 2881 cm^{-1} is due to CH_2 stretching mode and two bands at 1467 cm^{-1} and 1340 cm^{-1} attributed to the scissoring and wagging vibrations of CH_2, respectively. The CH_2 twisting vibrations are seen at 1278 cm^{-1} and 1240 cm^{-1}. The FT-IR bands found at 1144 cm^{-1}, 1097 cm$^{-1,}$ and 1060 cm^{-1} are assigned to the stretching vibration mode of C-O-C bonds. The stretching vibration of C-C and the bending vibration of CH_2 are located at 960 cm^{-1}. The IR bands at 870 cm^{-1} and 841 cm^{-1} are attributed to the bending vibration mode of C-O and the rocking mode of CH_2, respectively and the bending mode of the C-O-C bonds appeared at 530 cm^{-1} and 480 cm^{-1} [16-18]. The FT-IR bands of pure CMC polymer (spectrum b) appeared at 3288 cm^{-1} due to the stretching vibration of the O-H group and the small humps found at 2920 cm^{-1} and 2864 cm^{-1} are assigned to the stretching vibrations mode of CH_2. The sharp band located at 1587 cm^{-1} is due to the stretching vibration of the carboxyl group in the CMC. Two IR bands appear at 1412 cm^{-1} and 1323 cm^{-1} corresponding to the twisting and bending modes of CH_2 and O-H function groups, respectively and the stretching vibration modes of C-O-C are seen at 1053 cm^{-1} and 1020 cm^{-1} [19-21]. The spectrum c of pure $NiFe_2O_4$ depicts the main IR band at 580 cm^{-1} assigned to the metal-oxygen bond and confirmed the formation of $NiFe_2O_4$ NPs [22, 23].

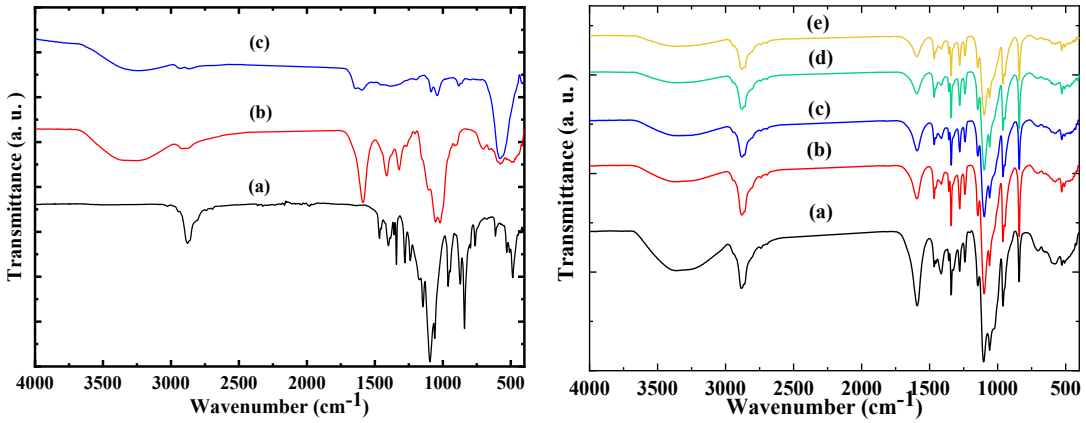

Fig. 1. ATR-FTIR of (a) PEO, (b) CMC and (c) $NiFe_2O_4$ NPs.

Fig. 2. shows the FT-IR spectrum of the pure PEO/CMC blend which shows a shift for the IR bands at 1587 cm^{-1}, 1097 cm$^{-1,}$ and 480 cm^{-1} toward the higher range of the wavenumber. Also, Bands at 1053 cm^{-1} and 870 cm^{-1} disappeared. In addition, there is an observable change in the intensity of all bands. This confirmed the chemical interaction and links between PEO and CMC polymers takes place because of the presence of O-H, and COO^- groups in the CMC and C-O-C groups of PEO polymer.

There is an observable decrease in the O-H band for PEO/CMC after being embedded by NiFe2O4 NPs. Also, it is a broadening increase with the addition of $NiFe_2O_4$ NPs. There is a shift in the band at 1103 cm^{-1} toward lower frequency, and the band 1323 cm^{-1} is disappeared. Also, all band intensities are decreased with the addition of $NiFe_2O_4$ NPs, this is due to the interaction between the PEO/CMC blend with $NiFe_2O_4$ nanoparticles.

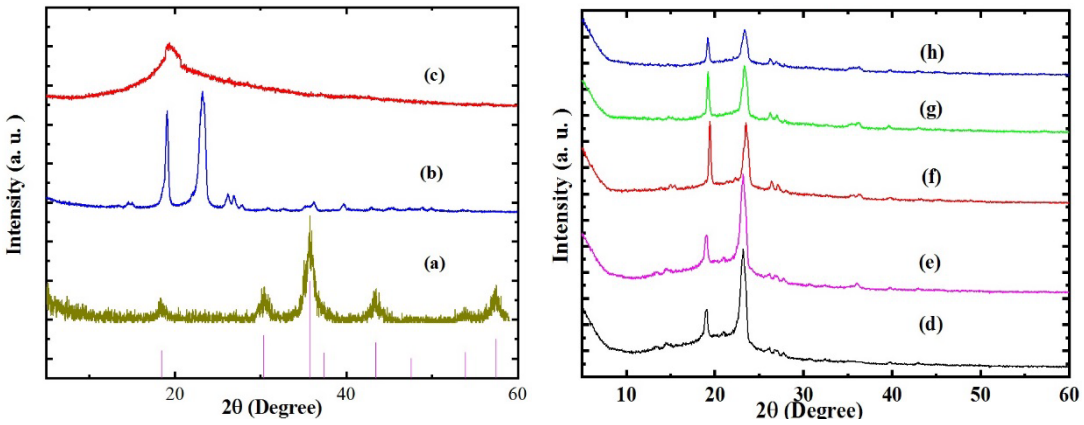

Fig. 2. ATR-FTIR of (a) PEO/CMC and PEO/CMC filled with (b) 4 wt.%, (c) 6wt.%, (d) 10 wt.% and (e) 15 wt.% $NiFe_2O_4$ NPs.

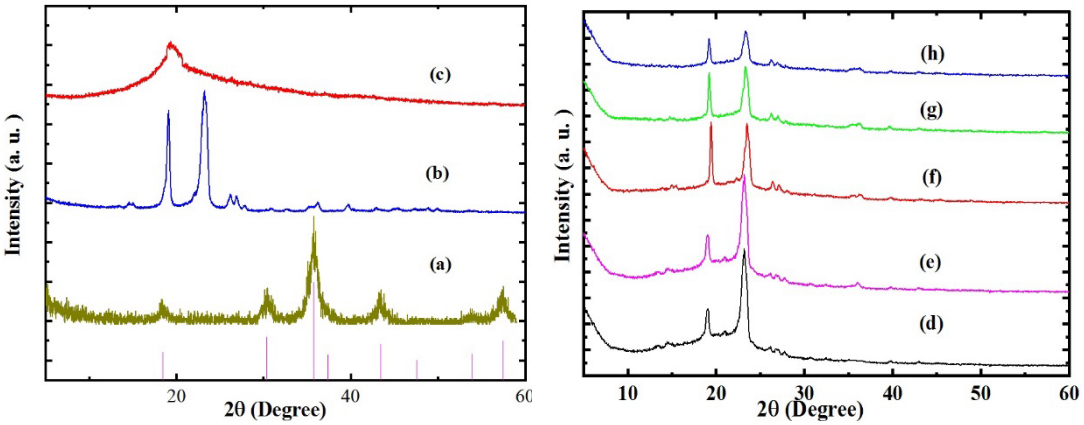

Fig. 3. XRD of (a) $NiFe_2O_4$ NPs, (b) PEO, (c) CMC, (d) PEO/CMC and PEO/CMC filled with (e) 4 wt.%, (f) 6wt.%, (g) 10 wt.% and (h) 15 wt.% $NiFe_2O_4$ NPs.

3.2. The X-ray diffraction (XRD)

Fig. 3a. illustrates the X-ray diffraction of pure $NiFe_2O_4$ NPs, pure PEO, and pure CMC in the range of 2θ = 5: 80 and Fig. 3b. PEO/CMC and PEO/CMC doped with different contents of $NiFe_2O_4$ NPs. As observed, $NiFe_2O_4$ NPs have diffraction peaks at 2θ = 18.2º, 30.4º, 35.7º, 43.4º and 57.4º which are due to (111), (220), (311), (400), and (511) lattice plane, respectively according to card no. 01-086-2267. The average crystal size of the prepared $NiFe_2O_4$ NPs deduced from the Scherrer formula [24]

$$S= 0.9\lambda/ \beta\cos\theta \quad (1)$$

where S is the crystallite size and λ is the X-ray wavelength. θ is the diffraction angle and β full width at half maximum of diffraction peak (FWHM). The average crystal size was determined and found to be 7 nm.

PEO has two main characteristic peaks at 2θ = 19.1º and 23.2º and other small peaks at 2θ = 26.1º, 26.8º, 27.7º, 36.2º and 39.7º according to previous literature [25], while CMC has a broad diffraction peak at 19.2º [26]. For PEO/CMC polymer blend diffraction pattern, it is observed that the crystalline nature of PEO is prominent and exhibited two main diffraction peaks at 2θ = 19.0º and 23.2º and other small diffraction peaks with low intensity at 2θ = 26.1º, 26.9º and 27.7º. This affirmed the interaction between PEO and CMC polymer, which agreed with previous literature [27].

For PEO/CMC embedded with different contents of $NiFe_2O_4$ NPs, the intensities of the two intrinsic peaks at 2θ = 19.0º and 23.2º have been arbitrarily reduced, and the increase in the content of amorphous phases can be seen in both the most recent samples (10 wt.% and 15 wt.% $NiFe_2O_4$ NPs). This decrease in crystallinity implies that the degree of crystallinity of PEO/CMC is disrupted due to the coordination interactions between the $NiFe_2O_4$ NPs and the PEO/CMC polymer blend. Also, these two peaks are shifted toward a higher theta degree, indicating that all$NiFe_2O_4$ NPs have been evenly distributed throughout the virgin polymer PEO/CMC. These findings suggest that $NiFe_2O_4$ NPs embedded within virgin PEO/CMC structure. They also offer the electrostatic interaction of this nanofiller with the polymer matrix (PEO/CMC) disrupts the crystalline sections of the matrix. These coordination interactions will be highlighted in the FTIR measurements.

3.3. UV-Vis analysis

Fig. 4. shows the UV-Vis spectrum of PEO/CMC and PEO/CMC incorporated by varying amounts of $NiFe_2O_4$ NPs. As observed in Fig. 4. PEO/CMC shows an absorption peak at 202 nm related to the n-π* transition due to the C=O chromophore [28]. For PEO/CMC embedded with different contents of $NiFe_2O_4$ NPs, the absorption peak at 202 nm is shifted toward a longer wavelength. Also, the absorption edge is shifted to the longer wavelengths with increasing $NiFe_2O_4$ NPs content.

The study of optical absorption can shed light on the band structure of organic materials. The only time that light absorption can take place is when an electron can transition from a lower energy state to a higher energy state by consuming a certain amount of energy in the form of photons. Changes in the amount of absorbed radiation can be used to identify the many kinds of electronic transitions that may take place. An abrupt change in the fundamental absorption can be understood as what is meant by the term "absorption edge." A relative rate of decrease in light intensity is indicated by the absorption coefficient (α) [29]:

$$\alpha = \frac{2.303}{d} A \tag{2}$$

where A is the absorbance and d is the thickness of the films. Fig. 5a represents the relation between the absorption coefficient (α) and photon energy ($h\upsilon$). As observed, with increasing $NiFe_2O_4$ NPs content, the absorption edge shifted toward lower photon energy depicting a decrease in band gap energy see Table .

The width of the defect bands that arise in the PEO/CMC-$NiFe_2O_4$ nanocomposites can be calculated as an intermediate state in the band gap, as it exhibits a band tail that extends from the bottom of the conduction band to the depth of the band gap, similarly, defect states that are very close to the valence band deformation also occurs at the edge of the valence band is deep inside a gap.

Urbach energy (E_u) is the name given to the energy connected to the defective tail, this is the Urbach tail [30].

$$\alpha = \alpha_0 \exp\left(\frac{h\upsilon}{E_u}\right) \tag{3}$$

The Urbach energy can be determined by plotting lnα vs. $h\upsilon$ as seen in Fig. 5b. The value of E_u can be determined by taking the reciprocal of the slopes of the linear part below the optical band gap. As seen in Table 1. the calculated values of the Urbach energy increased as an increase in $NiFe_2O_4$ NPs content. When the band gap gets smaller, the defect energy will get bigger. This

provides compelling evidence supporting our contention that forming sub-band states in the region between the conduction bands and the valence bands can reduce the values of the energy band gap.

The band gap energy (E_g) can be estimated from UV-Vis spectra according to the following relation [31]

$$(\alpha h\upsilon) = \varphi\,(h\upsilon - E_g)^{1/n} \quad (4)$$

Φ is assumed to be a constant and let the number of detectable transitions, n, be n equal 2 for direct transitions and n equal 1/2 for indirect transitions, respectively. Fig.6 displays the plot between $(\alpha h\upsilon)^2$ and $(\alpha h\upsilon)^{1/2}$ with hυ. The values of the direct and indirect band gaps are obtained by extrapolating the linear portion of the plot of $(\alpha h\upsilon)^2$ and $(\alpha h\upsilon)^{1/2}$ and versus photon energy to hv = 0. The direct and indirect band gap values are recorded in Table 1. It was demonstrated that $NiFe_2O_4$ NPs might reduce the direct and indirect band gaps compared to the PEO/CMC blend. This is likely owing to defects in the polymeric chain, which creates localized states in the energy gap and may be understood in the context of charge transfer complexes formed between the $NiFe_2O_4$ NPs dopant and the PEO/CMC blend. As the concentration of $NiFe_2O_4$ NPs rises, the overlapping and spreading of these localized states is observed. Because of this, doping with $NiFe_2O_4$ NPs increases the degree of disorder in the PEO/CMC blend.

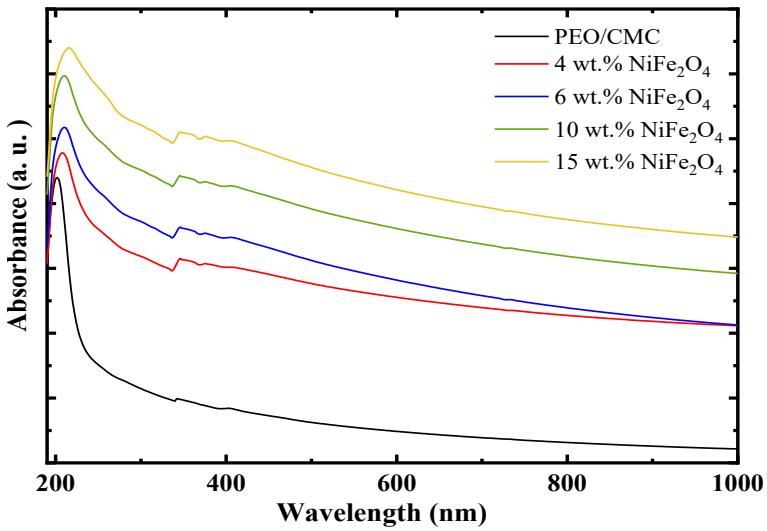

Fig. 4. UV-Vis of PEO/CMC /$NiFe_2O_4$ nanocomposites.

Table 1. Values of absorption edge, Urbach energy, and direct and indirect band gap energy of PEO/CMC/ $NiFe_2O_4$ nanocomposites.

$NiFe_2O_4$ Wt. %	Absorption edge (eV)	Band Tail E_u (eV)	Direct energy gap E_u (eV)	Indirect energy gap E_u (eV)
0	4.79	1.05	5.34	4.20
4	3.38	2.54	4.59	2.74
6	2.06	3.03	4.13	1.73
10	1.89	3.10	3.77	1.05
15	0.79	5.41	3.60	0.69

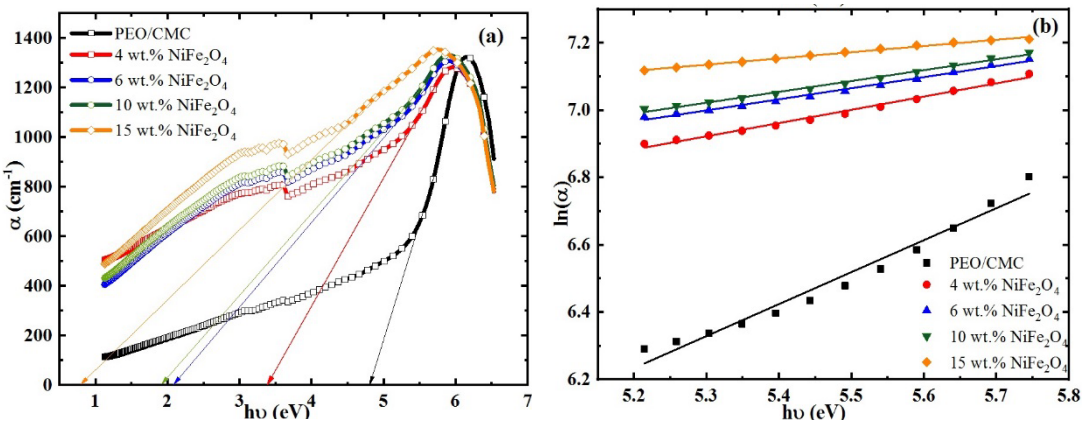

Fig. 5. Relation between α and ln α against hυ of PEO/CMC /$NiFe_2O_4$ nanocomposites.

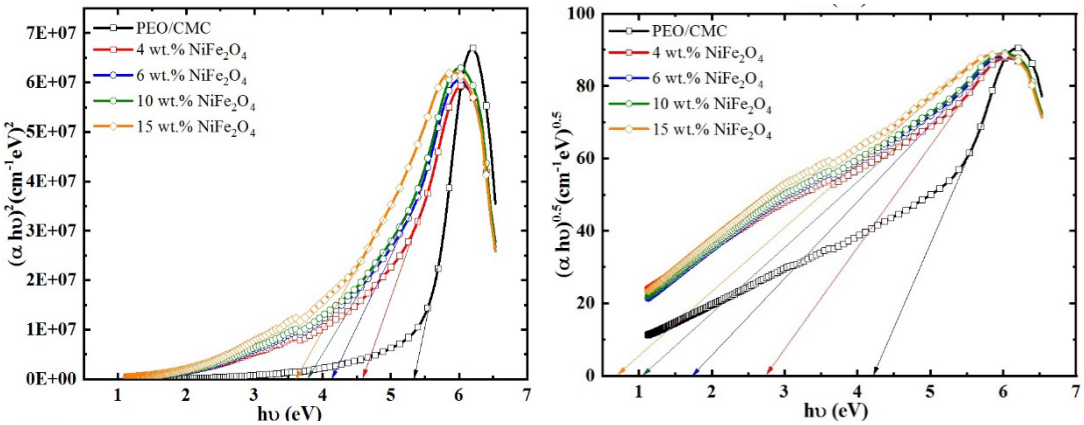

Fig. 6. Relation between $(\alpha h\upsilon)^2$ and $(\alpha h\upsilon)^{1/2}$ against hυ of PEO/CMC /$NiFe_2O_4$ nanocomposites.

3.4. Transmission electron microscope (TEM)

Fig. 7 provided TEM of $NiFe_2O_4$ NPs, as observed, the prepared $NiFe_2O_4$ NPs have a semispherical shape. According to statistical analysis, as depicted in the histogram of Fig. 7. the particles' diameter lies within the 3-9 nm range.

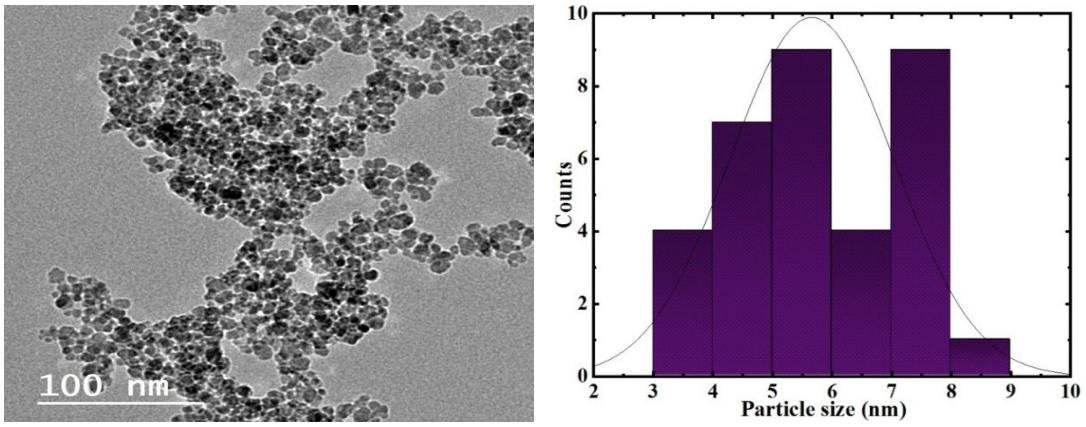

Fig. 7. TEM images and histogram of $NiFe_2O_4$ NPs.

3.5. Field-emission scanning electron microscopy (FESEM) and Energy Dispersive X-Ray (EDX)

Fig. 8. represents FESEM images and EDX analysis of $NiFe_2O_4$ NPs. The surface morphology of $NiFe_2O_4$ NPs. The $NiFe_2O_4$ NPs have a spherical shape and EDX analysis confirmed the formation of $NiFe_2O_4$ NPs.

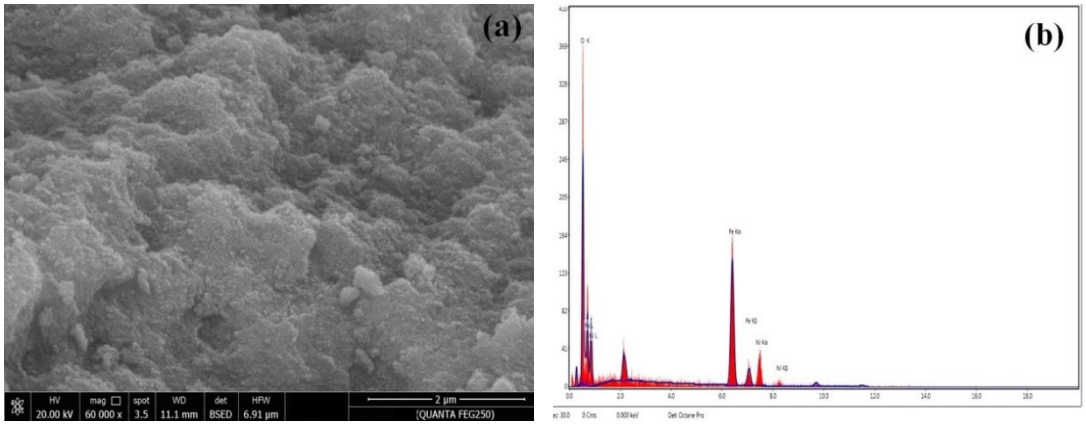

Fig. 8. FESEM and EDX analysis of $NiFe_2O_4$ NPs.

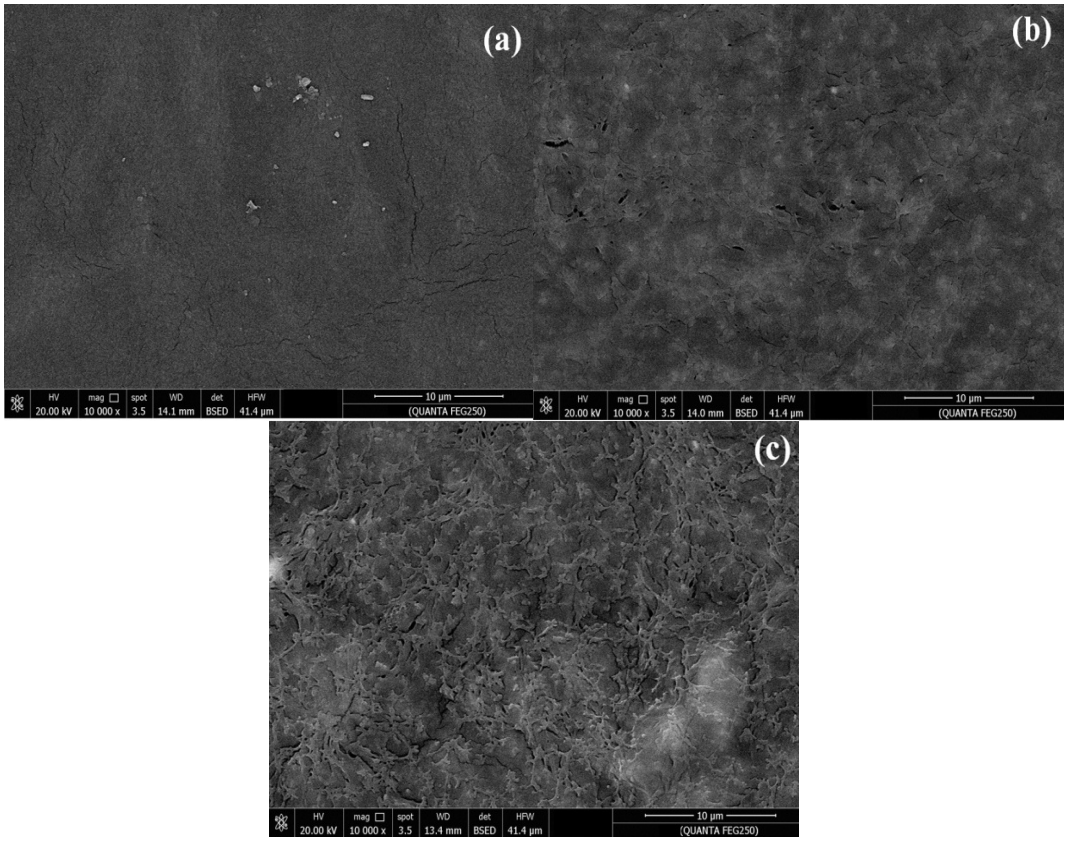

Fig. 9. FESEM of (a) PEO/CMC, (b) PEO/CMC/ 6wt.% $NiFe_2O_4$ NPs and (c) PEO/CMC/ 15wt. % $NiFe_2O_4$ NPs.

Fig. 9. represents FESEM of PEO/CMC, PEO/CMC/ 6wt.% $NiFe_2O_4$ NPs and PEO/CMC/ 15wt. % $NiFe_2O_4$ NPs. Fig. 9a. shows that the surface of PEO/CMC is smooth and homogenous. As the content of $NiFe_2O_4$ NPs increases, the surface roughness increases and the surface has a wrinkled

shape. The roughness of the surface is studied using Gwyddion software. As seen in Fig. 10.the mean roughness is 61.8 nm, 65.4 nm and 90.5 nm for PEO/CMC, PEO/CMC/ 6wt. % $NiFe_2O_4$ NPs and PEO/CMC/ 15wt. % $NiFe_2O_4$ NPs, respectively. Also, the mean square roughness is 78.6 nm, 81.4 nm, and 115.7 nm for PEO/CMC, PEO/CMC/ 6wt. % $NiFe_2O_4$ NPs and PEO/CMC/ 15wt. % $NiFe_2O_4$ NPs, respectively. This means that the surface area increases, making it useful in various applications.

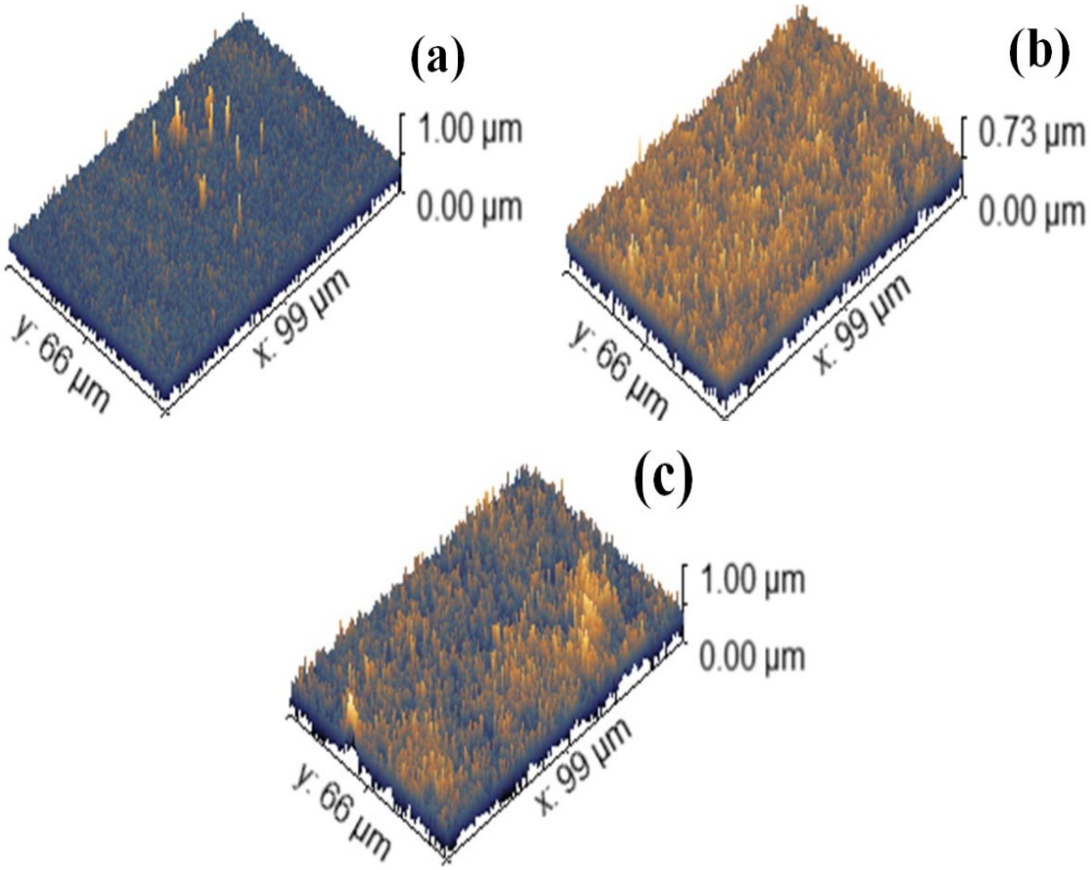

Fig. 10. 3D images of (a) PEO/CMC, (b) PEO/CMC/ 6wt.% $NiFe_2O_4$ NPs and (c) PEO/CMC/ 15wt. % $NiFe_2O_4$ NPs.

3.6. Dielectric studies

As an example, the Debye relation can be used to investigate the complex permittivity (ε*), the dielectric constant (ε'), and the dielectric loss (ε'') as shown in the relation [32].

$$\varepsilon^* = \varepsilon' - i\varepsilon'' \tag{5}$$

Fig. 11. shows the plot of ε' and ε'' with frequency. The dielectric constant is a function in capacity according to the formula $\varepsilon' = Cd/\varepsilon_0 A$ where ε' is a function of capacitance (C), A is the electrode area, d is the sample thickness, and ε_0 is the permittivity of free space. In addition, it was found that the dielectric constant exhibited non-Debye behavior, meaning that it decreased at the lower range of the frequencies. The plot shows that the polarization effects are responsible for a systematic decrease as the frequency increases.

Fig.11. depicts the relationship that exists between the frequency of the samples that have been prepared and the dielectric loss. As frequency increases, the behavior of ε'' degrades because space charges are unable to support and comply with the external field, leading to polarization generated by the ionic exchange of some ions by locally dispersing in the direction of the applied field. Ionic exchange locally displaced ions in the applied field to achieve this polarization. As the

frequency of the PEO/CMC-$NiFe_2O_4$ nanocomposite samples rises, the dipole will stop rotating and the oscillation will lag behind the applied field.

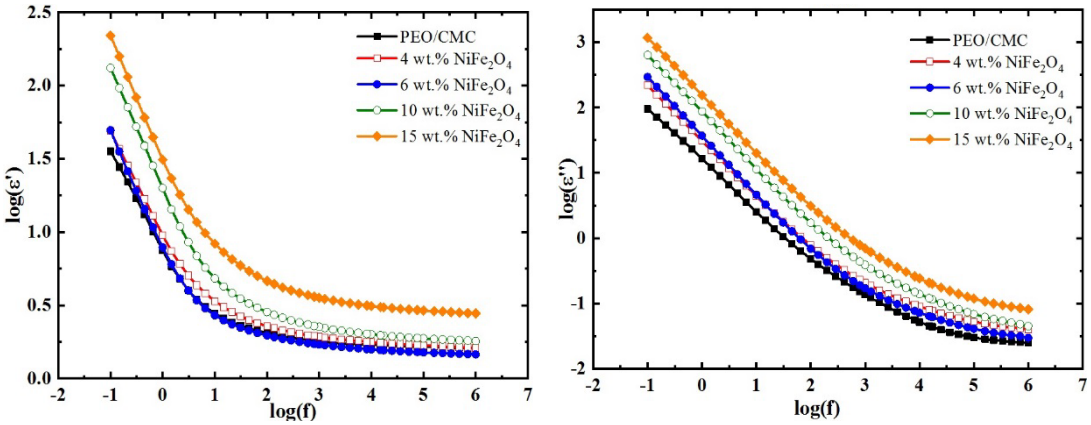

Fig. 11. Relation between dielectric loss and dielectric constant against frequency of PEO/CMC/ $NiFe_2O_4$ nanocomposites.

The values of ε' and ε'' for PEO/CMC-$NiFe_2O_4$ nanocomposite samples are higher than PEO/CMC polymer matrix due to the interactions between components causing an increase in the effective parallel ordering of dipoles cussing to improve in the dielectric polarization in the nanocomposites (after adding of $NiFe_2O_4$).

Fig. 12 represents all samples' conductivity against log (f) at room temperature. The conductivity is low at low-frequency levels due to interfacial impedance or space charge polarization. This indicates that the films that have been researched have non-Debye properties. The value of conductivity increases with increasing frequency. In addition to this, it was discovered that the conductivity values of PEO/CMC-$NiFe_2O_4$ nanocomposite were found to be higher in comparison to PEO/CMC, which indicates that the addition of $NiFe_2O_4$ NPs to the PEO/CMC may improve the mechanism of charge conduction in a slightly faster manner. Additionally, this enhancement may indicate a rise in the degree of disorder that limits the mobility of charge carriers and reveals the formation of an interconnected percolating chain suitable for charge transfer mechanisms [33].

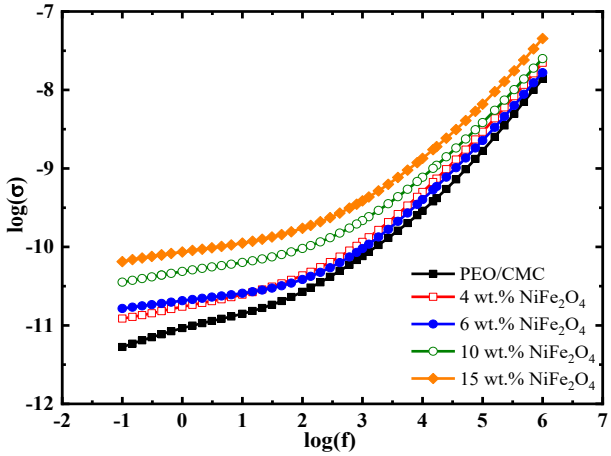

Fig. 12. Relation between Ac conductivity against frequency of PEO/CMC/ $NiFe_2O_4$ nanocomposites.

Fig. 13 illustrates the relationship between each sample's real component (M') and the imaginary part (M"). The curves represent the creation of a semicircle shape, which is consistent with the existence of extensive relaxation processes. The existence of one semicircle shows the relevance of single relaxation within the obtained samples, and the little of radius semicircles are associated with the largest capacitance in the PEO/CMC/ $NiFe_2O_4$ nanocomposites. It can be observed that with increasing $NiFe_2O_4$ NPs, the peak's semicircle nature is reduced, indicating an increase in the conductivity [34]. As seen in Fig. 13. the predominant relaxation peak detected in the middle-frequency range of the M" spectra can be attributed to interfacial polarization resulting from the accumulation of free charges at the interfaces of the polymer. This procedure is affected by the heterogeneity and conduction properties of the sample.

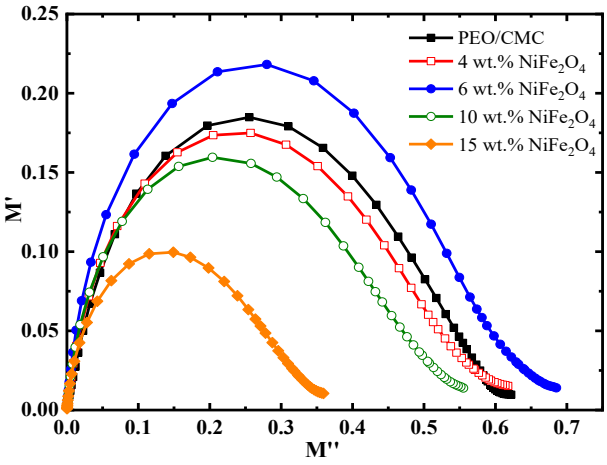

Fig. 13. Cole-Cole plot PEO/CMC/ $NiFe_2O_4$ nanocomposites.

4. Conclusions

Polymer nanocomposite films were prepared by the casting process where added different contents of nickel ferrite nanoparticles ($NiFe_2O_4$ nanoparticles to polyethylene oxide (PEO) and carboxymethyl cellulose (CMC) (50:50 wt%). The $NiFe_2O_4$ NPs which were prepared using solvothermal-produced formed by the XRD and ATR-FTIR, and TEM and demonstrated that they were semispherical with an average particle size of ~3-9 nm. The ATR-FTIR and XRD confirmed the miscibility and complexation between PEO/CMC as a pure blend and also between the blend with $NiFe_2O_4$ NPs. Changes in PEO/CMC-$NiFe_2O_4$ nanocomposites were observed to be structurally, optically, and morphologically.

The direct band gap energy value decreased from (5.34 to 3.6 eV) and the indirect band gap energy decreased from (4.2 to 0.69 eV) attributed to the absorption edge moving toward shorter wavelengths. The FESEM and 3D images revealed that the surface roughness increases with the addition of $NiFe_2O_4$ nanoparticles to the polymer blend. The AC electrical conductivity (σ_{ac}), dielectric constant (ε'), dielectric loss (ε''), and dielectric modulus (M', M") were measured between 0.1 Hz and 106 Hz. The values of σ_{ac} increase due to an increase in free charge density and charges mobility. as frequencies increased, both ε' and ε'' decreased. The plot between M' and M" reveals the semicircular form discussed according to a non-Debye model.

References

[1] Li, J., Zivanovic, S., Davidson, P. A., Kit, K. Carbohydrate Polymers, 79(3), 786-791. (2010); https://doi.org/10.1016/j.carbpol.2009.09.028

[2] Morsi, M. A., Abdelghany, A. M., Materials Chemistry and Physics, 201, 100-112. (2017); https://doi.org/10.1016/j.matchemphys.2017.08.022

[3] Choudhary, S. Structural, Journal of Physics and Chemistry of Solids, 121, 196-209. (2018); https://doi.org/10.1016/j.jpcs.2018.05.017

[4] Sahraeian, R., Davachi, S. M., Heidari, B. S., Composites Part B: Engineering, 162, 103-111. (2019); https://doi.org/10.1016/j.compositesb.2018.10.093

[5] Cha, J., Kim, J., Ryu, S., Hong, S. H., Composites Part B: Engineering, 162, 283-288. (2019); https://doi.org/10.1016/j.compositesb.2018.11.011

[6] Čech Barabaszová, K., Holešová, S., Bílý, M., Hundáková Journal of Inorganic and Organometallic Polymers and Materials, 30(10), 4218-4227. (2020); https://doi.org/10.1007/s10904-020-01573-y

[7] Jia, F., Liu, H. J., Zhang, G. G., Procedia Environmental Sciences, 31, 98-102. (2016); https://doi.org/10.1016/j.proenv.2016.02.013

[8] Gupta, B., Agarwal, R., Sarwar Alam, M., Journal of applied polymer science, 127(2), 1301-1308. (2013); https://doi.org/10.1002/app.37665

[9] Rajeh, A., Morsi, M. A., Elashmawi, I. S., Vacuum, 159, 430-440. (2019); https://doi.org/10.1016/j.vacuum.2018.10.066

[10] Tongdeesoontorn, W., Mauer, L. J., Wongruong, S., Sriburi, P., Rachtanapun, P., Chemistry Central Journal, 5(1), 1-8. (2011); https://doi.org/10.1186/1752-153X-5-6

[11] Abdelghany, A. M., Abdelrazek, E. M., Badr, S. I., Morsi, M. A., Materials & Design, 97, 532-543. (2016); https://doi.org/10.1016/j.matdes.2016.02.082

[12] Hassen, A. M. E. S., El Sayed, A. M., Morsi, W. M., El-Sayed, S., Journal of Applied Physics, 112(9), 093525. (2012); https://doi.org/10.1063/1.4764864

[13] Naidu, T. M., Narayana, P. L., Journal of Nanoscience and Technology, 769-772. (2019); https://doi.org/10.30799/jnst.247.19050407

[14] Joshi, S., Kumar, M., Chhoker, S., Srivastava, G., Jewariya, M., Singh, V. N., Journal of Molecular structure, 1076, 55-62. (2014); https://doi.org/10.1016/j.molstruc.2014.07.048

[15] Yan, J., Huang, Y., Chen, X., Wei, C., Synthetic Metals, 221, 291-298. (2016); https://doi.org/10.1016/j.synthmet.2016.09.018

[16] Sim, L. H., Gan, S. N., Chan, C. H., & Yahya, R. J. S. A. P. A. M., Spectrochimica Acta Part A: Molecular and Biomolecular Spectroscopy, 76(3-4), 287-292. (2010); https://doi.org/10.1016/j.saa.2009.09.031

[17] Abdelrazek, E. M., Abdelghany, A. M., Badr, S. I., Morsi, M. A., Research Journal of Pharmaceutical. Biol. Chem. Sci, 7, 1877-1890. (2016).

[18] Abd El-kader, F. H., Hakeem, N. A., Hafez, R. S., Ismail, A. M., Journal of Inorganic and Organometallic Polymers and Materials, 28(3), 1037-1048. (2018); https://doi.org/10.1007/s10904-017-0763-x

[19] Vitamin, P., Malaysian Journal of Analytical Sciences, 19(1), 275-283. (2015).

[20] Rozali, M. L. H., Ahmad, N. H., Isa, M. I. N., American-Eurasian Journal of Sustainable Agriculture. (2015).

[21] Mondal, M. I. H., Yeasmin, M. S., Rahman, M. S., International Journal of Biological Macromolecules, 79, 144-150. (2015); https://doi.org/10.1016/j.ijbiomac.2015.04.061

[22] Asiri, S., Sertkol, M., Güngüneş, H., Amir, M., Manikandan, A., Ercan, İ., Baykal, A., Journal of Inorganic and Organometallic Polymers and Materials, 28(4), 1587-1597. (2018); https://doi.org/10.1007/s10904-018-0813-z

[23] Elashmawi, I. S., Ismail, A. M., Polymer Bulletin, 1-20. (2022); https://doi.org/10.1007/s00289-022-04139-9

[24] Patterson, A., The Physical Review, 56(10), 978-982. (1939); https://doi.org/10.1103/PhysRev.56.978

[25] Abd El-kader, F. H., Hakeem, N. A., Hafez, R. S., Ismail, A. M., Journal of Inorganic and Organometallic Polymers and Materials, 28(3), 1037-1048. (2018); https://doi.org/10.1007/s10904-017-0763-x

[26] Guo, X., Chen, N., Meng, X., Wang, X., Li, Y., Xie, Q., IOP Publishing. (2019, November); https://doi.org/10.1088/1757-899X/678/1/012115

[27] Tarabiah, A. E., Alhadlaq, H. A., Alaizeri, Z. M., Ahmed, A. A., Asnag, G. M., Ahamed, M., Journal of Polymer Research, 29(5), 1-16. (2022); https://doi.org/10.1007/s10965-022-03011-8

[28] Morsi, M. A., Abdelaziz, M., Oraby, A. H., Mokhles, I., Journal of Materials Science: Materials in Electronics, 29(18), 15912-15925. (2018); https://doi.org/10.1007/s10854-018-9677-9

[29] Elashmawi, I. S., Hakeem, N. A., Polymer Engineering & Science, 48(5), 895-901. (2008); https://doi.org/10.1002/pen.21032

[30] Choudhury, B., Dey, M., Choudhury, A., International Nano Letters, 3(1), 1-8. (2013); https://doi.org/10.1186/2228-5326-3-25

[31] Elashmawi, I. S., Al-Muntaser, A. A., Journal of Inorganic and Organometallic Polymers and Materials, 31(6), 2682-2690. (2021); https://doi.org/10.1007/s10904-021-01956-9

[32] Baskaran, R., Selvasekarapandian, S., Hirankumar, G., Bhuvaneswari, M. S., Ionics, 10 (1), 129-134. (2004); https://doi.org/10.1007/BF02410321

[33] Hafez, R. S., Hakeem, N. A., Ward, A. A., Ismail, A. M., Abd El kader, F. H., Journal of Inorganic and Organometallic Polymers and Materials, 30(11), 4468-4480. (2020); https://doi.org/10.1007/s10904-020-01637-z

[34] Farea, M. O., Abdelghany, A. M., Oraby, A. H., RSC advances, 10 (62), 37621-37630. (2020); https://doi.org/10.1039/D0RA07601E